Nucleic Acids Research, 2025, **53**, gkaf017
https://doi.org/10.1093/nar/gkaf017
Advance access publication date: 24 January 2025
Chemical Biology and Nucleic Acid Chemistry

Proximity-activated guide RNA of CRISPR–Cas12a for programmable diagnostic detection and gene regulation

Zhian Hu[1,*,†], **Shen Ling**[1,†], **Jialin Duan**[1,†], **Zixiao Yu**[1], **Yanfei Che**[1], **Song Wang**[1], **Sichun Zhang**[2], **Xinrong Zhang**[2], **Zhengping Li**[1,*]

[1]Beijing Key Laboratory for Bioengineering and Sensing Technology, University of Science and Technology Beijing, Beijing 100083, China
[2]Department of Chemistry, Tsinghua University, Beijing 100084, China

*To whom correspondence should be addressed. Email: zhianhu@ustb.edu.cn
Correspondence may also be addressed to Zhengping Li. Email: lzpbd@ustb.edu.cn
†The first three authors should be regarded as Joint First Authors.

Abstract

The flexibility and programmability of CRISPR–Cas technology have made it one of the most popular tools for biomarker diagnostics and gene regulation. Especially, the CRISPR–Cas12 system has shown exceptional clinical diagnosis and gene editing capabilities. Here, we discovered that although the top loop of the 5′ handle of guide RNA can undergo central splitting, deactivating CRISPR–Cas12a, the segments can dramatically restore CRISPR function through nucleic acid self-assembly or interactions with small molecules and aptamers. This discovery forms the basis of an engineered Cas12a system with a programmable proximity-activated guide RNA (PARC–Cas12a) that links targets of interest to dsDNA. Leveraging the efficient *trans*- and *cis*-cleavage of Cas12, our findings further inspired a detection platform design for RNAs or non-nucleic acid biomarkers, enabling highly sensitive and multiplexed analysis. We further demonstrated the feasibility of RNA-controllable gene knockout/knockdown in *Escherichia coli*. Notably, we successfully validated the gene regulatory capabilities of the PARC–Cas12a system within mammalian cell systems by utilizing the classical theophylline molecule–aptamer system. Our results introduce a programmable toolbox for precise diagnostics and cell regulation, allowing the development of versatile diagnostic tools, complex synthetic biological circuits, and cellular biosensors.

Graphical abstract

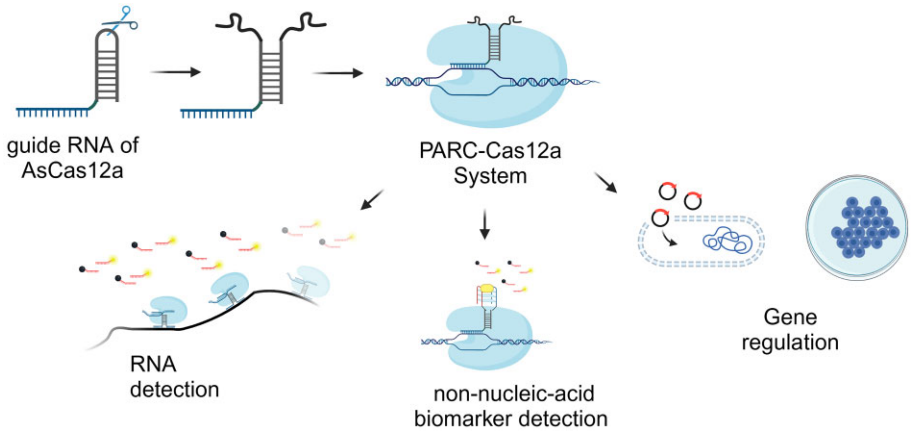

Introduction

In recent years, CRISPR–Cas (clustered regularly interspaced short palindromic repeats–CRISPR-associated proteins) systems have emerged as one of the most crucial tools for gene engineering, continuously pushing the boundaries of possibility in genetic research and applications [1–3]. CRISPR–Cas systems, including CRISPR–Cas9, CRISPR–Cas12, and CRISPR–Cas13 systems, are complexes comprising a Cas protein and a guide RNA (gRNA) to identify and cleave genomic DNA or RNA sequences [4]. Intriguingly, RNA engineering modules, such as aptamers and riboswitches combined with gRNAs, have been applied to overcome key bottlenecks and propel the advancements of synthetic biology, theranostics, and biocomputing [5, 6]. The CRISPR–Cas12 system, especially Cas12a from *Acidaminococcus* species, known as AsCpf1, is among the most extensively engineered CRISPR–Cas sys-

Received: December 12, 2024. **Revised:** January 3, 2025. **Editorial Decision:** January 4, 2025. **Accepted:** January 8, 2025

tems used for the development of human therapeutics and precision diagnostics [2, 7, 8]. Both Cas12a and Cas9 efficiently induce double stranded DNA (dsDNA) breaks via gRNA-mediated gene editing. Cas12a, however, has a lower off-target rate than Cas9, which is a compact protein structure and targets "TTTN" protospacer adjacent motif (PAM) sequences, whereas Cas9 targets guanine (G)-rich PAM sequences [9]. Additionally, a distinctive feature of Cas12a is its *trans*-cleavage activity, which involves the nonspecific cleavage of single-stranded DNA (ssDNA) with high catalytic turnover [10]. By leveraging this ability, researchers have developed many molecular diagnostic tools capable of detecting trace amounts of nucleic acid biomarkers [11–14]. We envision that integrating RNA engineering modules within the gRNA of the CRISPR–Cas12a could lead to a highly efficient signal processing system that enables more precise control of cellular behavior by chemical or biochemical stimuli, and sensing the interest of nucleic acid and non-nucleic acid targets.

Compared with the gRNA of other CRISPR systems, the gRNA of Cas12a is highly conserved and compact [15]. The CRISPR–Cas12a functions in cooperation with a gRNA, consisting of a 5′ handle (~20 nucleotides) and a guide segment (21–25 nucleotides) [16]. Cas12a protein interacts tightly with the pseudoknot structure formed by the 5′ handle sequence. Li *et al*. conducted a detailed study on the engineering potential of the gRNA for Cas12a [17]. Owing to the high conservation of the 5′ handle, the addition, deletion, or modification of the chemical bases in this region can lead to significant inhibition of the CRISPR–Cas12a activity [18]. Thus, the development of CRISPR–Cas12a-based RNA engineering strategies has inherent limitations. To date, the functionalization of the Cas12a gRNA has been achieved mostly by strand replacement strategies in the spacer region or the 5′ handle region [11, 19, 20]. Although strand displacement is useful, the trigger RNA sequence is strictly limited by the 5′ handle and spacer sequences, as well as by the hairpin secondary structure of the RNA, requiring rigorous design [21, 22].

Improving the CRISPR technique requires the exploration of flexible and simple RNA engineering strategies with superior performance [6, 23, 24]. Our group has performed extensive research on the structure of the AsCpf1–gRNA complex and successfully modified the gRNA for controllable gene regulation [25]. We observed that the 5′ handle of Cpf1 was positioned in a pocket-like domain and that the top-loop sequence (UCUU) of the 5′ handle was exposed on the exterior surface of the Cas protein, forming an "isolated" small loop (Fig. 1A). Intriguingly, in this work, we found that while a break in the "UCUU" sequence can lead to the loss of CRISPR activity, through nucleic acid self-assembly or RNA–small molecule interactions, the newly formed RNA fragments can be religated and CRISPR–Cas12a activity can be restored. On this basis, we further constructed an engineered CRISPR–Cas12a system with a programmable proximity-activated guide RNA (PARC–Cas12a) (Fig. 1B). In *in vitro* experiments, we thoroughly explored the characteristics of the PARC–Cas12a system. By utilizing the highly efficient *trans*-cleavage ability of Cas12a, we successfully developed a highly sensitive and preamplification-free RNA detection strategy. Besides, by utilizing the flexible programmable capability of PARC–Cas12a, a multiplex detection platform was demonstrated for the simultaneous analysis of 10 RNA samples in a single test. Inspired by our biochemical results, we further verified the suitability of an RNA-controllable PARC–Cas12a system for genetic cleavage and regulation in prokaryotic cells. More importantly, by modifying the "UCUU" sequence and structure, we successfully incorporated gene regulatory elements, such as the MS2 hairpin motif, in mammalian cells for transcriptional regulation. By integrating RNA aptamer technology with the PARC–dCas12a system, we verified a small molecule-regulated CRISPR tool, enabling precise control of gene expression in mammalian cells. This flexible system could be broadly useful for many applications in CRISPR-mediated chemical and biological engineering.

Materials and methods

The structure information of AsCas12a (PDB: 5B43) was downloaded from www.rcsb.org. The structure of gRNA and its variants were predicted by *Snapgene* software.

RNA and DNA preparation

The single-strand oligo and RNAs were purchased from GenScript (Nanjing, China) and Sangon Biotech Co., Ltd (Shanghai, China). These commercial nucleic acids were purified by high-performance liquid chromatography (HPLC) without RNase and DNase, and characterized by matrix-assisted laser desorption–ionization time-of-flight mass spectrometry (MALDI–TOF MS) or electrospray mass spectrometry (ESI-MS). The dsDNA in Supplementary Table S4 was synthesized by gene synthesis services of GenScript. Besides, we obtained long-chain RNA such as crTheo (see sequence in Supplementary Table S1) using *in vitro* transcription. The RNA was transcribed using the Takara *in vitro* Transcription T7 Kit. The ssDNA template with the T7 promoter was first heated to 65°C and then added to the mixture including T7 RNA polymerase and transcription buffer for an overnight reaction at 42°C. DNase I (Takara, 2270B) was added according to the instructions to digest the ssDNA template. The RNA product was purified using the Fast RNA Column Purification Kit (Sangon Biotech, Shanghai) and characterized by 15% denaturing polyacrylamide gel electrophoresis (PAGE) (65°C, 130 V, and 45 min).

The *cis*-cleavage and *trans*-cleavage reaction *in vitro*

For *cis*-cleavage, 100 ng of dsDNA activator (sequence in Supplementary Table S1) is added to a 200 μl of a centrifuge tube. Then, gRNA (100 nM), 0.4 μg of Cas12a protein, and 2 μl of Cas12a reaction buffer [10×: 500 mM NaCl, 100 mM Tris–HCl, 100 mM $MgCl_2$, 1 mg/ml bovine serum albumin (BSA), pH 7.9] were added to the tube. For inducible PARC–Cas12a, the trigger substances [trigger RNA, adenosine triphosphate (ATP), and theophylline] were mixed with gRNA and Cas protein together. After that, deionized water without DNase and RNase was quickly added to mixture with 20 μl total volunm. The centrifuge tube was placed in a polymerase chain reaction (PCR) instrument and incubated at 37°C for 2 h for the cleavage reaction. After the reaction, 10 μg of Proteinase K was added and the mixture was incubated at 55°C for 30 min to digest the Cas protein and terminate the reaction. The cleavage products were characterized by agarose gel electrophoresis (1%). Note that the concentrations of Cas12a, gRNA, and dsDNA activator need to be optimized for the best experimental results.

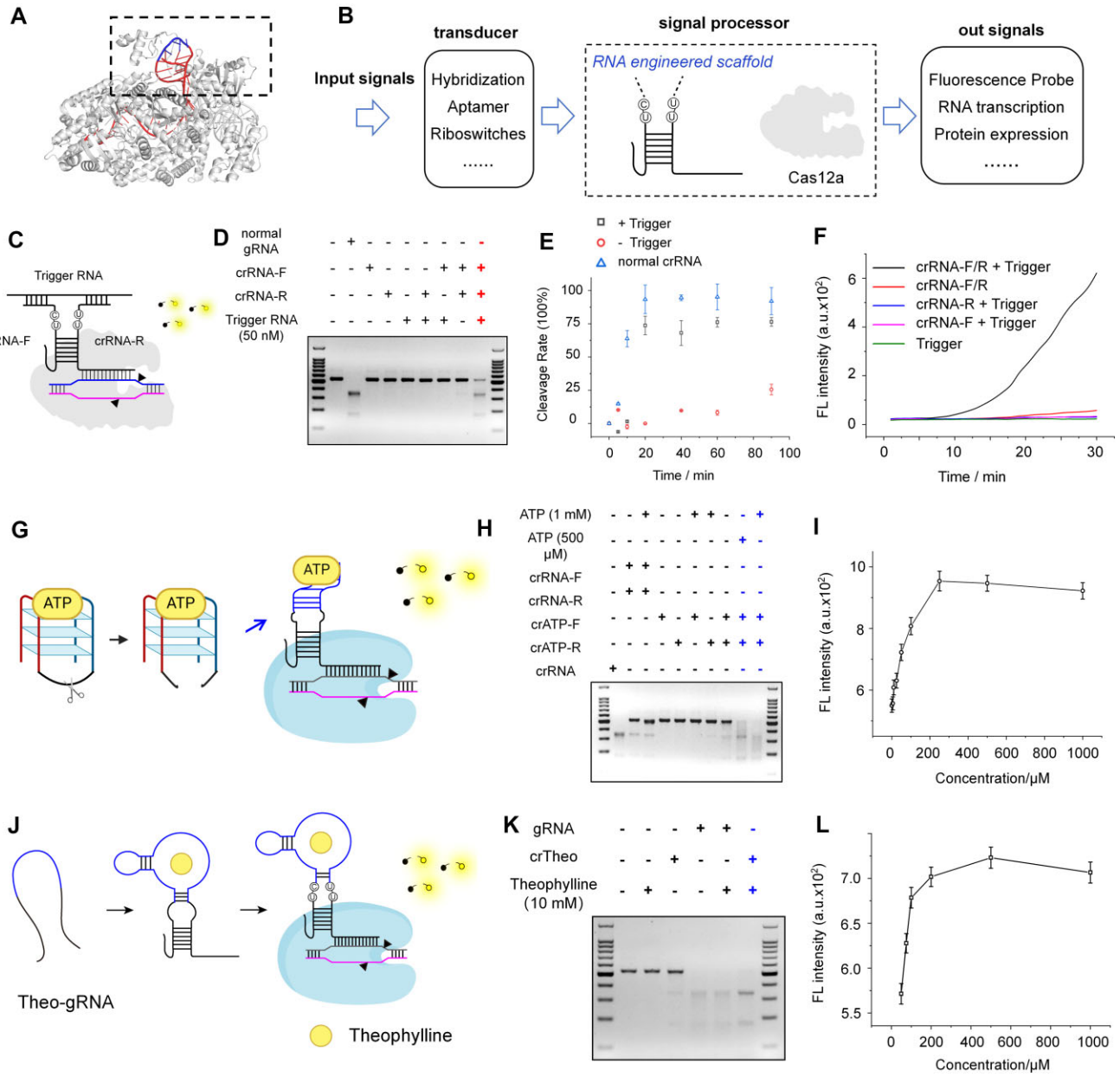

Figure 1. Programmable PARC–Cas12a system. (**A**) Crystal structure overview of AsCas12a and the gRNA. (**B**) Conversion of various input signals into specific output signals (such as fluorescence, protein products, or RNA transcription) through the PARC–Cas12a system. (**C**) RNA-inducible PARC–Cas12a system. (**D**) Feasibility test of *cis*-cleavage. The reactions were conducted at 37°C for 2 h, and the products were further characterized by agarose gel electrophoresis (1%). (**E**) The *cis*-cleavage time course of the RNA-inducible PARC–Cas12a system with a trigger RNA concentration of 50 nM. (**F**) The *trans*-cleavage fluorescent time course of the RNA-inducible PARC–Cas12a system with a trigger RNA concentration of 50 nM. (**G**) Structures formed by the binding of ATP to a DNA aptamer (left) and split DNA aptamers (right). Performance of the ATP-inducible PARC–Cas12a. (**H**) The feasibility of *cis*-cleavage ability by the ATP-inducible PARC–Cas12a system. (**I**) ATP concentration-dependent (1000, 500, 250, 100, 50, 25, 10, 5, and 0 μM) *trans*-cleavage activity of PARC–Cas12a. (**J**) Schematic diagram of the theophylline-inducible PARC–Cas12a system. (**K**) The products of theophylline-inducible PARC–Cas12a *cis*-cleavage were characterized via agarose gel (1%). (**L**) The theophylline concentration-dependent (1000, 500, 200, 100, 75, and 50 μM) *trans*-cleavage activity of Cas12a. DNA ladder (top to bottom): 1500, 1000, 900, 800, 700, 600, 500, 400, 300, 200, and 100 bp. Error bars represent the standard deviation of three measurements.

For the *trans*-cleavage assay, the sequence of the FQ probe was listed in Supplementary Table S1 (5′-modified 5-Carboxyfluorescein (FAM) and 3′-modified Black Hole Quencher 1 (BHQ1)). The gRNA (100 nM), Cas12a protein (0.4 μg), FQ probe (500 nM), and ssDNA activator (50 nM) or dsDNA activator (100 ng) were mixed into 200 μl of the PCR tube in order, added into 1 μl of Cas12a reaction buffer (10×: 500 mM NaCl, 100 mM Tris–HCl, 100 mM $MgCl_2$, 1 mg/ml BSA, pH 7.9), and quickly brought the total volume to 10 μl with DNase/RNase-free deionized water. As for inducible PARC–Cas12a, the trigger substances were mixed with gRNA and Cas protein together, and then the other reactants were added in the same order as described above. For fluorescent time-course detection, the mixture was transferred to a 384-well microtiter plate. It was excited at 488 nm, and the fluorescence intensity was monitored at 525 nm for ∼2 h us-

ing a SpectraMax iD3 microplate reader (Molecular Devices). For fluorescence spectra and intensity detection, the mixture was incubated on a PCR instrument at 37°C for 1 h, and then heated at 95°C for 10 min to terminate the cleavage reaction. The results were recorded using a Hitachi F-7000 fluorescence spectrometer. For the CRISPR–Cas13a detection, LbuCas13a (100 nM), CRISPR guide RNA (crRNA, 50 nM), FQ probe (500 nM), and 1× buffer (50 mM NaCl, 10 mM Tris–HCl, 10 mM $MgCl_2$, 100 μg/ml BSA, pH 7.9) were coincubated at 37°C, and the fluorescence was recorded by a microplate reader.

The analysis of electrophoretic mobility shift assay

Briefly, 8.3 ml of 30% (29:1 Acr/bis), 5 mM 10× Tris/Borate/EDTA (TBE) buffer, 36 ml of diethypyrocarbonate (DEPC)-treated H_2O, 0.6 ml of $Na_2S_2O_3$ (300 μg/ml), and 100 μl of Tetramethylethylenediamine (TEMED) were mixed in order. After 1 h, the PAGE gel was pre-electrophoresed at 200 V in 1× TBE for ∼30 min on ice. The FAM-labeled gRNA, Cas protein, and Cas12a reaction buffer were mixed into 9 μl of deionized water without DNase and RNase. Then, this mixture was incubated at 37°C for ∼45 min to form RNA and protein complex (RNP). RNPs (9 μl) were loaded onto gel with loading buffer [2.5× TBE and 40% (v/v) glycerol]. Finally, in a cooling bath, the gel was conducted at 120 V in 0.5× TBE for ∼0.5 h, and the results were pictured by the Typhoon™ FLA 9500 laser scanner.

The multiplex RNA detection based on streptavidin magnetic bead–dsDNA metal probe strategy

The sequences of DMPs, crRNA-F, crRNA-R, and RNA samples are listed in Supplementary Tables S2–S5. The protocol for combining the DMPs to streptavidin-coated magnetic beads (SMBs) was based on Dynabeads™ M-280 Streptavidin's instructions. Briefly, 100 μl of SMBs (∼6×10^7) were mixed with biotin-labeled dsDNA metal probes (DMPs, 10 μM) and incubated at room temperature for 30 min. The supernatant was separated using a magnetic rack (DynaMag-2), and the beads were washed three times with PBST buffer (1× PBS and 0.01% Tween 20) to obtain the metal-labeled magnetic beads. For multiplex RNA detection, different metal-labeled DMPs were bound to SMBs to obtain various metal-labeled magnetic beads. Depending on the target RNA sequence, the corresponding DMP-labeled magnetic beads (∼10^5) were mixed to create a probe mixture solution. After that, Cas12a (4 μg), crRNA-F (50 nM), crRNA-R (50 nM), and the RNA samples were mixed and incubated at room temperature for 30 min. Metal probe magnetic beads were then added to the mixture and reacted at 37°C for 1 h. The supernatant was collected and 500 μl of 1% HNO_3 was added for iCAP Q inductively coupled plasma mass spectrometry (ICP-MS) detection (Thermo Fisher, Germany; Re and Rh elements were used as internal standards). The parameters of the ICP-MS detection are listed in Supplementary Table S12.

The synthesis process of dsDNA metal probes

In a solution of 100 μM NH_2-modified ssDNA, a 40-fold excess of the metal-chelating 1,4,7,10-tetraazacyclododecane-1,4,7,10-tetraacetic acid mono-*N*-hydroxysuccinimide ester (DOTA-NHS) compound was added, and the reaction was allowed to proceed overnight at 37°C. After HPLC purification, the metal-modified ssDNA was annealed with the biotin-modified complementary strand to form the DMP.

Strains and plasmids

The *Escherichia coli* strain DH5α was used for plasmid cloning and grown in Luria–Bertani (LB) medium with suitable antibiotics. *Escherichia coli* strain MG1655 (close to wild-type bacteria) for testing our PARC-Cas12a/dCas12a system. The plasmid maps and gRNA sequences in this study were listed in Supplementary Tables S7–S10. For RNA-inducible PARC–Cas12a/dCas12a in *E. coli*, the AsCas12a or dAsCas12a gene sequences were synthesized by GenScript and directly cloned into a pACYC vector with chloramphenicol-resistant using NcoI and NdeI sites. The dAsCas12a (E993A) sequence was based on the plasmid from Addgene #102565 (AsCpf1), with the amino acid at position 993 mutated from E to A. The GFP gene was cloned from Addgene plasmid #23027 and inserted with the trc promoter and lac operator into the pET-15b vector, creating the ampicillin-resistant pET-GFP plasmid. The sfGFP and mRFP1 genes were directly synthesized by GenScript and inserted into the pSC101-TIMER backbone (Addgene #103057) at the BstBI and HindIII sites. The normal gRNA and split crRNA sequences were controlled by the constitutive J23119 promoter and poly(T)terminator. They were ligated into the PACYC-dAsCas12a (E993A) or PACYC-AsCas12a plasmid using restriction enzyme digestion and ligation. The DNA encoding the mammalian codon-optimized dAsCpf1 nuclease, harboring the inactivating D908A mutation, was based on Addgene plasmid (#86209, D908A) and cloned into a plasmid containing an EF-1α (Elongation Factor 1 Alpha) promoter, resulting in the plasmid dAsCas12a (D908A). The U6-gRNA-TRE-miniCMV-tagBFP plasmid, TRE-miniCMV-tagBFP plasmid, and tripartite VP64-P65AD-Rta (VPR) transcriptional activator plasmid were gifted by Xinrong Zhang's group. The MS2 coating protein (MCP) fused with Sun-Tag and the scFv-VP64 protein were both chemically synthesized by GenScript and cloned using the pEASY®-Basic Seamless Cloning and Assembly Kit to obtain the MCP-SunTag 10×, MCP-SunTag 24×, and scFv-sfGFP-VP64 plasmids.

RNA-inducible PARC–Cas12a system in *E. coli*

The spacer sequence was designed using the online tool at http://grna.ctegd.uga.edu/. The MG1655 strain cells were co-transformed with plasmids PACYC-Trigger 1 (expressing As-Cas12a, split gRNAs, and trigger RNA) and signal plasmid, such as pET-GFP (expressing green fluorescence protein (GFP)), by heat shock. The transformed MG1655 cells were then cultured in 3 ml of LB medium (10 g/l tryptone, 5 g/l yeast extract, and 10 g/l NaCl) supplemented with ampicillin (50 μg/ml) and chloramphenicol (25 μg/ml) for ∼24 h. The cells transfected with PACYC-no Trigger1 plasmid and pET-GFP plasmid were chosen as the control group. The culture cells were diluted 100-fold, and the fluorescence intensity was measured by the flow cytometry (CytoFLEX S, Beckman Coulter, China), and the data were collected from 10 000 bacteria. Total RNA was extracted from the culture, and 5 ng of total RNA was used for real-time quantitative PCR (qRT-PCR) analysis, following the Hifair® III One Step RT-qPCR SYBR Green Kit protocol.

For CRISPR interference (CRISPRi) target gene in *E. coli*, the experimental steps were basically the same as described above, with the AsCas12a protein replaced by dAsCas12a (E993A). The single colonies transfected with the plasmids were picked from agar plates and grown in LB medium with the corresponding plasmid resistance (Amp 50 μg/ml, Cmt 25 μg/ml, and KanR 100 μg/ml) at 37°C for >12 h. Total RNA was then extracted and analyzed by qRT-PCR, and the fluorescence could be directly recorded by a 96-well plate microplate reader (SpectraMax iD3 microplate reader) or flow cytometry.

Mammalian cells culture, transfection, and analysis

The HEK293T cell line was cultured in Dulbecco's Modified Eagle's Medium (DMEM) supplemented with 10% fetal bovine serum (FBS) and 100 IU/ml penicillin–streptomycin (PS) at 37°C under 5% CO_2 and split at a ratio 1:4 every 2 days in T25 culture flasks. The plasmids for CRISPRa in mammalian cells were cotransfected to cells by Hieff Trans™ Liposomal Transfection Reagent. Briefly, in a 12-well plate, HEK293T cells were grown to 70%–90% density. Then, 1 μg of each plasmid was premixed with 6 μl of transfection reagent for 20 min in 100 μl of Opti-MEM medium. The mixture was added to 1.5 ml of antibiotic-free DMEM (10% FBS), followed by a medium change to DMEM with 10% FBS and 100 IU/ml PS after 12 h of incubation. Further after 48 h, the cells were imaged by a laser confocal microscope (LeiCa-TCS SP8, Germany), and the imaging data were analyzed using ImageJ software. Besides, the fluorescence was recorded by flow cytometry (CytoFLEX S, Beckman Coulter, China), counting 10 000 cells as the stopping condition.

For mRNA (Messenger RNA) level analysis through qRT-PCR, the total RNA of transfected cells was obtained by MolPure® Cell RNA Kit (the number of cells was 10^5), and the extraction process was followed strictly according to the manufacturer's instructions. The RNA samples were quantified by NanoDrop 2000 (Thermo Fisher, USA) and further analyzed by qRT-PCR using Hifair® III One Step RT-qPCR SYBR Green Kit. The primers are listed in Supplementary Table S11, and the *GAPDH* was selected as the housekeeping gene.

Theophylline-inducible CRISPRa system in HEK293T cells

Similar cell culture procedures were followed as described above. For each well in a 12-well plate, 1 μg of dAsCas12a-VPR plasmid and 0.5 μg of U6-Theo/2A-TRE-miniCMV-tagBFP plasmid were transfected using 6 μl of Hieff Trans™ Liposomal Transfection Reagent. The mixture was added to 1.5 ml of antibiotic-free DMEM (10% FBS) and incubated for 12 h. A stock solution of 100 mM theophylline was prepared in 60 mM NaOH and added into 1.5 ml of DMEM with 10% FBS and 100 IU/ml PS to the cells for 12 h at the 8 mM concentration. The cells were harvested for 48 h after transfection and analyzed using a laser confocal microscope. Additionally, the fluorescence was recorded using a flow cytometer as described above.

Results

Design of the PARC–Cas12a system based on structural insights

From the structure of *Streptococcus pyogenes* Cas9 (SpCas9, PDB: 4OO8), it is obvious that multiple highly flexible hairpin structures exist when the gRNA binds to the Cas9 protein. In particular, the complete tetraloop domain of the gRNA protrudes outside the surface of the Cas protein. This domain is formed by the outward extension of the hybridized part of the tracrRNA and the crRNA, and is thus an optimal anchoring position for combining engineered RNA devices with the CRISPR–Cas9 system. We next examined the previously determined crystal structure of *Acidaminococcus* sp. Cas12a (AsCas12a) in complex with a gRNA and a complementary target DNA (Fig. 1A, PDB: 5B43). The loop region in the 5′ handle of the gRNA is positioned in an open pocket-like structure of the Cas12a protein, where the four bases "UCUU" (Fig. 1A, marked in blue) are completely free of interactions with the amino acid side chains of Cas12a. We splitted the gRNA at the central "UCUU" sequence and named the resulting fragments, crSplitF and crSplitR. Even when both fragments were incubated with the Cas protein, they failed to activate CRISPR–Cas12a as efficiently as the intact gRNA did (Supplementary Fig. S1A) to cleave the dsDNA target (Supplementary Fig. S2). The electrophoretic mobility shift assay (EMSA) results indicated that while crSplit-R retained some binding activity toward Cas12a, the binding activity of crSplit-F was significantly reduced (Supplementary Fig. S1B). In other words, by reassembling crSplit-F and crSplit-R into an artificial gRNA through external means, such as nucleic acid hybridization, Cas12a might be efficiently reactivated.

We further devised a trigger RNA and extended the 3′ end of crSplit-F and the 5′ end of crSplit-R (crRNA-F and crRNA-R) outward, allowing the three RNAs to form a stable T-shaped crossover (TC) tile to activate Cas12a (Fig. 1C). Since this assembly process takes place outside the Cas12a-binding domain, CRISPR–Cas12a activity should be affected only weakly by the TC tile. As expected, the dsDNA target was cleaved by the complex of Cas12a and the TC tile (Fig. 1D). The kinetic results further indicated that the trigger RNA exhibited a strong activating effect on Cas12a activity (Fig. 1E and Supplementary Fig. S3). The cleavage assay of the dsDNA indicated that the recognition arms of crRNA-F/R need to contain >13 nucleotides (nt) and have a T_m of >40°C (Supplementary Fig. S4). To determine whether the trigger RNA can activate the *trans*-cleavage of Cas12a, a single-stranded poly(T) sequence was designed with FAM at the 5′ end and BHQ1 at the 3′ end as the substrate (FQ probe). The results indicated that trigger RNA promoted the formation of TC tiles, thereby activating Cas12a to cleave the FQ probe, resulting in a significant increase in fluorescence (Fig. 1F).

We sought to determine whether the split gRNAs could be combined with aptamers to construct an attractive non-nucleic acid target-inducible PARC–Cas12a system. We began with the ATP aptamer because it is well studied [26]. In our design, the split gRNAs (crATP-F and crATP-R, Fig. 1G) are composed of DNA–RNA chimeras. We confirmed that the activity of our designed system was strictly dependent on the presence of ATP (Fig. 1H). By exploiting the *trans*-cleavage activity of Cas12a, we observed a distinct positive correlation

between the ATP concentration and the fluorescence intensity, with a strong linear relationship over the range 5–100 μM (Fig. 1I and Supplementary Fig. S5). The limit of detection (LOD) was determined to be 1.67 μM (LOD: the concentrations corresponding to a signal 3 SD above the mean of 11 replicates of the zero calibrator). Furthermore, selectivity assays demonstrated that the ATP-inducible PARC–Cas12a system displayed specificity against structurally similar interferents (Supplementary Figs S5 and S6).

Theophylline and mTCT8-4 are widely used in cellular regulation, logic gates, and biosensing applications [27]. However, the gel electrophoresis results revealed that even in the presence of high concentrations of theophylline (10 mM), the dsDNA cleavage activity of PARC–Cas12a could not be induced (Supplementary Fig. S7). We suspect that this failure may be due to the weaker affinity between theophylline and mTCT8-4 than between ATP and its G4 aptamer. Upon further consideration, we hypothesized that using mTCT8-4 to directly link the split gRNA fragments at the "UCUU" site to form a single Theo-gRNA could put the core sequence of the gRNA in a pseudo-split state (Fig. 1J). When theophylline is present, its interaction with the aptamer pulls the gRNA fragments together, promoting the proper folding and activation of Cas12a through a riboswitch mechanism. The results of the *in vitro* dsDNA cleavage assay demonstrated that theophylline molecules can function as a switch to regulate the activity of PARC–Cas12a (Fig. 1K). The theophylline aptamer maintained its specificity even when incorporated into the gRNA (Supplementary Fig. S8B and C). In addition, the cleavage activity of Cas12a was positively correlated with the concentration of theophylline in the system (Fig. 1L). Overall, our data provide proof of principle for a non-nucleic acid target-inducible PARC–Cas12a *in vitro* system and introduce two activation strategies: direct aptamer splitting and the riboswitch mechanism. Via our strategy, we can repurpose the PARC–Cas12a system into a universal sensor for the detection of a broad spectrum of non-nucleic acid targets and nucleic acid targets.

The programmed split gRNA enables highly sensitive and multiplex RNA detection for diagnostics

We next evaluated the RNA quantification ability of the PARC–Cas12a system. Notably, the fluorescence signal increased proportionally with the trigger RNA concentration (Fig. 2A). We next compared the RNA detection ability between the LbuCas13a system and the RNA-inducible PARC–Cas12a system. The LOD of PARC–Cas12a system is 11.2 pM. Our established system is comparable to LbuCas13a (LOD ~ 6.21 pM), and the LODs of both are in the pM range. Notably, the PARC–Cas12a system cleaves DNA, whereas the CRISPR–Cas13a system directly recognizes and degrades the target RNA. The RNA target remained intact for up to 1 h after recognition by the PARC–Cas12a system (Fig. 2C). Leveraging this unique advantage, we proposed a highly sensitive RNA detection strategy based on PARC–Cas12a array (arrayPARC–Cas12a). We used the N-gene SARS-CoV-2 RNA as sample (Supplementary Table S6). Since PARC–Cas12a does not degrade RNA samples, it is theoretically possible to design a series of split-crRNA groups to construct an N-gene SARS-CoV-2 mRNA detection array, forming a structure analogous to single-molecule fluorescence *in situ* hybridization (Fig. 2D) [28, 29]. This RNP array can leverage the signal amplification capability of Cas12a, significantly enhancing the sensitivity of RNA detection. We compared the Cas13a array with the PARC–Cas12a array, as shown in Fig. 2E. The Cas13a, due to its RNA degradation activity, could only support 2–3 Cas13a–crRNA RNPs, which is a critical limitation for high-sensitivity RNA sample detection. In contrast, the SARS-CoV-2 mRNA detection was able to accommodate >10 sets of PARC–Cas12a detection arrays, achieving a remarkable sensitivity of 10 fM in solution within 30 min (Fig. 2F). Overall, PARC–Cas12a could be a highly sensitive RNA detection platform.

Given the excellent capabilities of the PARC–Cas12a system for RNA recognition, DNA recognition, and DNA cleavage, we sought to determine the feasibility of developing a single-tube method for a multiplex RNA assay. For proof the concept, gel electrophoresis was employed to decode the cleavage products from the pool of dsDNA targets (Supplementary Fig. S9A). We selected specific mRNA fragments from seven common viruses. Seven dsDNA substrates were designed with the FAM fluorophore at the 5′ end, ensuring the presence of one visualizable product on the gel. As expected, the gel electrophoresis results demonstrated that the cleavage of the seven RNA targets produced dsDNA fragments with different lengths (Supplementary Fig. S9B). In general, accurate and highly sensitive quantification of multiplex RNA samples, even with >10 RNAs in a single analysis, remains challenging. Fluorescence-based strategies are limited by spectral overlap. The ICP-MS has become a powerful tool for quantitative analysis of metal in materials science and biology [30]. To fully actualize the multiplexing potential of the PARC–Cas12a system, we designed a multiplex RNA assay using DMPs and SMBs. This approach leverages the capabilities of PARC–Cas12a for precise recognition and efficient cleavage, employs metal elements for multiplex labeling, uses magnetic microparticles for rapid separation, and utilizes the ICP-MS for accurate multiplex detection (Fig. 2G). The DMPs were synthesized under mild conditions by NH_2-labeling DNA coupled with metal-chelated DOTA-NHS and characterized by MALDI-TOF MS (Fig. 2H and Supplementary Figs S10–S12). We expanded the assay to detect 10 common viral mRNAs. In this assay, each RNA fragment was identified by measuring the m/z spectrum of its uniquely labeled rare earth elements. Figure 2I and F shows the ICP-MS results for mixtures containing 10 RNA samples at three different concentrations (5, 50, and 500 fmol). These results indicate that, owing to the PARC–Cas12a system, the concentration of the RNA samples is directly proportional to the signal intensity of the rare earth metals determined by the ICP-MS (Supplementary Fig. S14). Notably, the ICP-MS can distinguish most isotopes of metal elements (Supplementary Fig. S13), suggesting that the DMP-SMB strategy could be used for the simultaneous quantitative analysis of over 10 RNA species in a single assay.

Regulation of gene expressions via RNA-inducible PARC–Cas12a in *E. coli*

Among the designs previously mentioned, the RNA-inducible PARC–Cas12a system has considerable promise for synthetic biology applications, particularly in versatile gene circuits. We first tested the suitability of the system for inducible gene knockout in *E. coli* (Fig. 3A). In our design, three components were required: the AsCas12a protein with nuclease activity, a

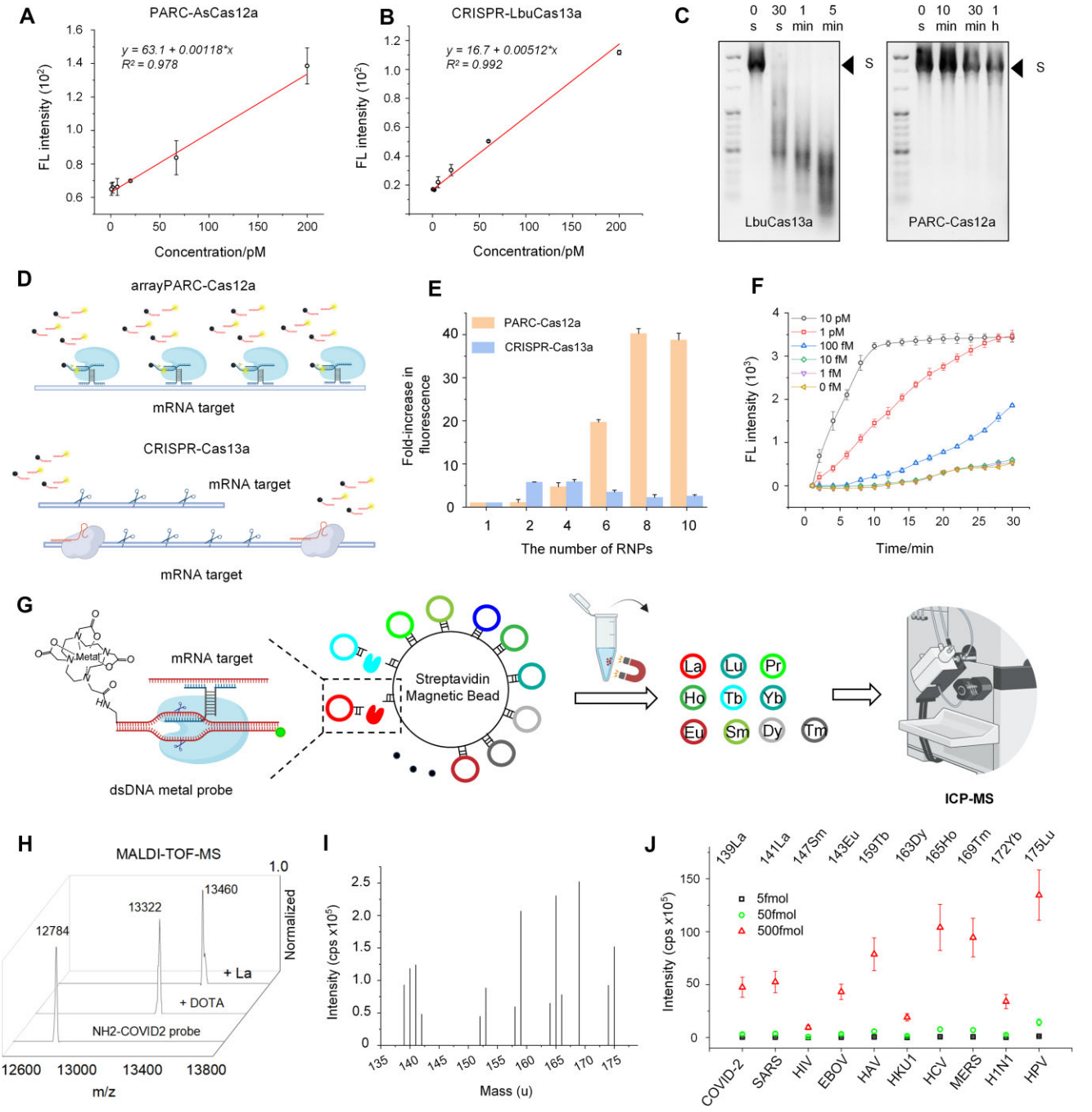

Figure 2. RNA detection based on PARC–Cas12a system. (**A** and **B**) Calibration curves plotting the fluorescence intensity versus COVID-2 mRNA concentrations using the PARC–Cas12a system and CRISPR–Cas13a (60 nM, 20 nM, 6 nM, 2 nM, 600 pM, and 200 pM). (**C**) The time-dependent cleavage results of mRNA. (**D**) arrayPARC–Cas12a and classic Cas13a in RNA detection. (**E**) Comparation of the Cas13a array with the PARC–Cas12a array in signal amplification. (**F**) Detection of SARS-CoV-2 N-gene RNA with 10 RNPs of arrayPARC–Cas12a. (**G**) Quantification of multiplex RNAs based on the SMB–DMPs strategy. (**H**) MALDI–TOF MS characterization of DNA-labeled metal elements. The *m/z* of NH_2-modified DNA was 12 784 *m/z*. The *m/z* of DOTA conjugated DNA was 13 322, and that of La-labeled DNA was 13 460. (**I**) The ICP-MS spectrum of DMPs labeled with 14 metal isotopes (^{139}La, ^{140}Ce, ^{141}Pr, ^{144}Nd, ^{150}Sm, ^{152}Eu, ^{157}Gd, ^{159}Tb, ^{163}Dy, ^{165}Ho, ^{167}Er, ^{169}Tm, ^{173}Yb, and ^{175}Lu). (**J**) The ICP-MS spectra of 10 target viral RNA targets at three different concentrations (5, 50, and 500 fmol). The RNA samples were analyzed simultaneously. The error bars represent the standard deviation of three measurements.

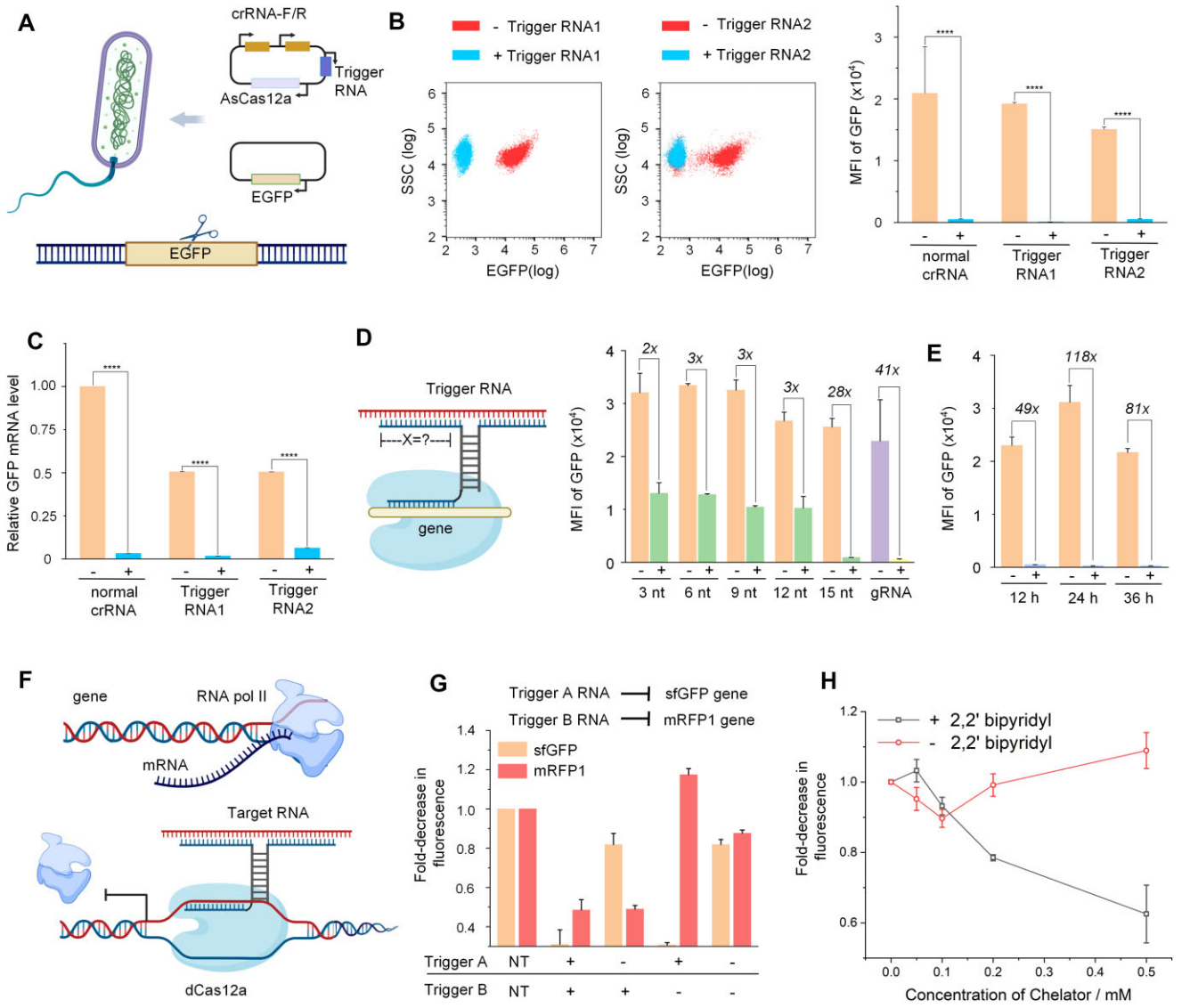

Figure 3. Performance of the RNA-inducible PARC–Cas12a system in *E. coli*. (**A**) Diagram showing the process for gene knockout by the RNA-inducible PARC–Cas12a system. (**B** and **C**) Flow cytometry and qRT-PCR were used to measure GFP expression in bacteria. The normal gRNA represents the gRNA without RNA engineering. "±" represents the conditions with or without trigger RNA. (**D**) Impacts of recognition arm length of the split gRNAs. "±" represents the conditions with or without Trigger RNA1. (**E**) Changes in GFP fluorescence in MG1655-GFP cells transfected with PACYC-Trigger 1 (+) or PACYC-no Trigger 1 (−) were measured at 12, 24, and 32 h. (**F**) Schematic diagram of the process for RNA-inducible CRISPRi in *E. coli*. (**G**) Multiplexed temporal control of the expression of two genes with two trigger RNAs based on the PARC–dCas12a system. NT denotes the nontargeting gRNA sequence (random sequences). The reporter fold change is defined as the fluorescence observed upon induction with the indicated trigger RNA (*x*-axis) divided by the fluorescence observed in the NT-gRNA group. (**H**) Fold-decrease in sfGFP fluorescence in response to varying concentrations of the chelator 2,2′-bipyridyl (0, 0.05, 0.1, 0.2, and 0.5 mM). "±" represents the in presence/absence of 2,2′-bipyridyl. The error bars represent the standard deviation of three measurements. ***$P < .001$ and ****$P < .0001$ were determined using Student's *t*-test.

target gene, and three RNAs for assembling the TC tile. To demonstrate this concept, we first generated *E. coli* MG1655 strains stably expressing GFP (Supplementary Fig. S15) and separately introduced artificial trigger RNAs into the bacteria cells via heat shock. The flow cytometry results indicated that Trigger RNA1 and Trigger RNA2 significantly reduced GFP fluorescence compared to the control (no trigger RNA) group (Fig. 3B). Furthermore, we measured the mRNA level of GFP via qRT-PCR, and the results were consistent with the flow cytometry findings (Fig. 3C). Afterward, we optimized the RNA recognition arm lengths of the split gRNAs in *E. coli*. We found that the recognition arm needed to contain at least 15 nt to result in a significant reduction in the GFP signal compared with that in the no trigger RNA group (Fig. 3D). These results were essentially consistent with those of the *in vitro* experiments (Supplementary Fig. S4). We then measured fluorescence via flow cytometry at 12, 24, and 32 h post-transfection. Significant GFP cleavage was observed as early as 12 h post-transfection with Trigger RNA1, resulting in a >40-fold reduction in GFP fluorescence compared with that in the no trigger RNA group (Fig. 3E and Supplementary Fig. S16).

Additionally, we expected that the PARC–dead Cas12a (dCas12a, lack DNase activity) system could also be used for multiplex gene regulation in *E. coli*. We replaced the AsCas12a protein with dAsCas12a (E993A). We constructed a plasmid coexpressing sfGFP and monomeric red fluores-

cent protein (mRFP1). We initially designed crRNA spacers for efficient CRISPRi targeting of sfGFP and mRFP1 (Supplementary Fig. S17). Then, Trigger-A and Trigger-B were designed to achieve CRISPRi in the sfGFP gene and mRFP1 gene, respectively (Supplementary Fig. S18A and B). As shown in Fig. 3G, Trigger-A and Trigger-B exhibited weak crosstalk, with sfGFP and mRFP1 being inhibited in the presence of their corresponding trigger RNA. In other words, the transcription of both genes can be regulated by the levels of the corresponding trigger RNA in *E. coli*. To expand the use of the PARC–dCas12a system for inducible endogenous gene knockdown, we designed a spacer for crRNA-R to target the coding region of the endogenous *lacZ* gene. The PARC–dCas12a system was introduced into the bacterial cells, and the *lacZ* mRNA level was measured via qRT-PCR. As expected, the presence of Trigger-C RNA effectively reduced the *lacZ* mRNA level, achieving an inhibition efficiency of ∼49.9% (Supplementary Fig. S18C). Furthermore, another key test involved the use of endogenous RNA as the trigger RNA to achieve inducible CRISPRi. The sRNA RyhB is a classic target to validate the performance of RNA-responsive CRISPR–Cas systems. The sRNA RyhB is highly expressed in low-iron environments, aiding bacterial in adaptation to iron-deficient conditions [31]. Generally, the addition of 2,2′-bipyridyl can reduce bacterial iron uptake, thereby increasing the expression levels of RyhB RNA (Supplementary Fig. S19). The 3′ fragment of crRyhB-F and the 5′ fragment of crRyhB-R were designed to target the sRNA RyhB sequence. The spacer for crRyhB-R was designed to target the sfGFP gene, As expected, low concentrations of the iron chelator did not lead to significant changes in sfGFP fluorescence. However, at a 2,2′-bipyridyl concentration of 0.5 mM, iron deficiency led to high expression of RyhB RNA, activating CRISPRi and reducing the sfGFP fluorescence intensity to ∼50% of the level observed under nonstressed conditions (Fig. 3H). These results highlight the feasibility of using the RNA-inducible PARC–Cas12a system in prokaryotic cells. Importantly, the selection of the trigger RNA and gene of interest is mutually independent. Through the rational design of split gRNAs and trigger RNA sequences, our strategy can be extended for the design of more complex genetic circuits and the sensing endogenous RNAs.

Performance of the PARC–Cas12a system in HEK293T cells

Compared with the bacteria, mammalian cells exhibit substantially increased internal complexity. CRISPR–RNA engineering in mammalian cells remains a considerable challenge. Here, we first attempted to introduce a hairpin aptamer at the "UCUU" site of the gRNA to investigate its impact on Cas12a activity, employing the MS2 aptamer, which can bind to the MS2 bacteriophage coat protein [32]. We applied the CRISPR activation (CRISPRa) system to test the activity of the MS2 aptamer–gRNA (MS2–gRNA) in HEK293 cells (Fig. 4A). The dCas12a protein, which lacks DNase activity, was fused to a tripartite VPR transcriptional activator [25]. When the gRNA binds to dAsCas12a–VPR, the complex targets the TRE promoter region, activating the transcription of tagBFP driven by the miniCMV promoter. The intensity of the blue fluorescence and the number of fluorescent HEK293 cells effectively reflect the activity of MS2–gRNA. Unexpectedly, directly embedding the MS2 aptamer at the "UCUU" split site did not result in observable blue fluorescence in cells (Fig. 4 and Supplementary Fig. S20). We next added nucleotides between the MS2 aptamer and the gRNA as a "lubricant" to improve the compatibility of MS2–gRNA with the Cas protein (Supplementary Fig. S23). Interestingly, adding three adenine (A) bases as a linker slightly increased the activity of MS2–gRNA, as evidenced by the appearance of cells exhibiting blue fluorescence, whereas the addition of uracil (U), guanine (G), or cytosine (C) base had almost no effect on MS2–gRNA activity (Supplementary Fig. S20). Surprisingly, when two adenine bases were used as a linker, the activation efficiency of MS2–gRNA peaked, reaching up to 50% of that of the normal gRNA (Fig. 4B and C). Additionally, the flow cytometry and qRT-PCR results were consistent with the observations made via the confocal microscopy (Fig. 4D and Supplementary Fig. S21). The PP7 stem–loop and its coat protein interaction are analogous to the corresponding features of the well-studied MS2 bacteriophage system and are widely used in RNA engineering in eukaryotic cells [33]. Remarkably, adenine bases demonstrated a "lubricating effect," with constructs containing a single adenine base as a linker retaining a most of 35% of gRNA activity (Fig. 4E).

We next envisioned the construction of a robust signal-responsive PARC–Cas12a system for controllable gene regulation in mammalian cells (Fig. 5A). The secondary structure of the theophylline aptamer (mTCT8-4) is highlighted within the black dashed box in Supplementary Fig. S22, with the theophylline recognition domain enclosed in the blue box. Stem1 is tightly linked to the "UCUU" region of the gRNA, whereas Stem2 enhances the stability of the theophylline aptamer. Consequently, we attempted to embed the mTCT8-4 aptamer into the "UCUU" site to enlarge the loop of the 5′ handle, thereby inactivating the CRISPR–Cas12a system. For the proof of concept, the dAsCas12a–VPR plasmid and the TRE-miniCMV-tagBFP reporter plasmid were employed, and the activity of the PARC–Cas12a system was monitored by detecting the fluorescence signal of tagBFP. Additionally, we added two adenine bases as a linker to bridge the gRNA and mTCT8-4 aptamer to improve the compatibility of the Cas protein and gRNA (resulting in Theo-2A-gRNA; Fig. 5D and Supplementary Fig. S22). As expected, the presence of Theo-2A-gRNA along with theophylline significantly increased the fluorescence intensity of tagBFP. In contrast, when theophylline was not present or when the spacer for Theo-2A-gRNA was replaced with a random RNA sequence, the system exhibited low background activity comparable to that of a negative control system lacking a guide RNA (Fig. 5B and C). The CRISPRa activity of Theo-2A-gRNA was further assayed by confocal imaging at 72 h after transient transfection. The efficiency of the Theo-2A-gRNA-activated CRISPR–Cas12a system gradually increased with the increasing theophylline concentrations over the concentration range of 0 to 8 mM range (Fig. 5D). These meaningful results prompted us to further assess the regulation of endogenous genes by the theophylline-inducible PARC–Cas12a system. To this end, we designed four spacers targeting the promoter regions of DNA (cytosine-5)-methyltransferase 1 (*DNMT1*) and interleukin 1 receptor antagonist (*IL1RN*) on both the target and nontarget strands. Approximately 24 h after transient transfection of the relevant plasmids into HEK293 cells, 4 mM theophylline was added, and the cells were cultured for an additional 48 h before collection. The qRT-PCR results revealed increased transcription of the target genes in these cells compared to

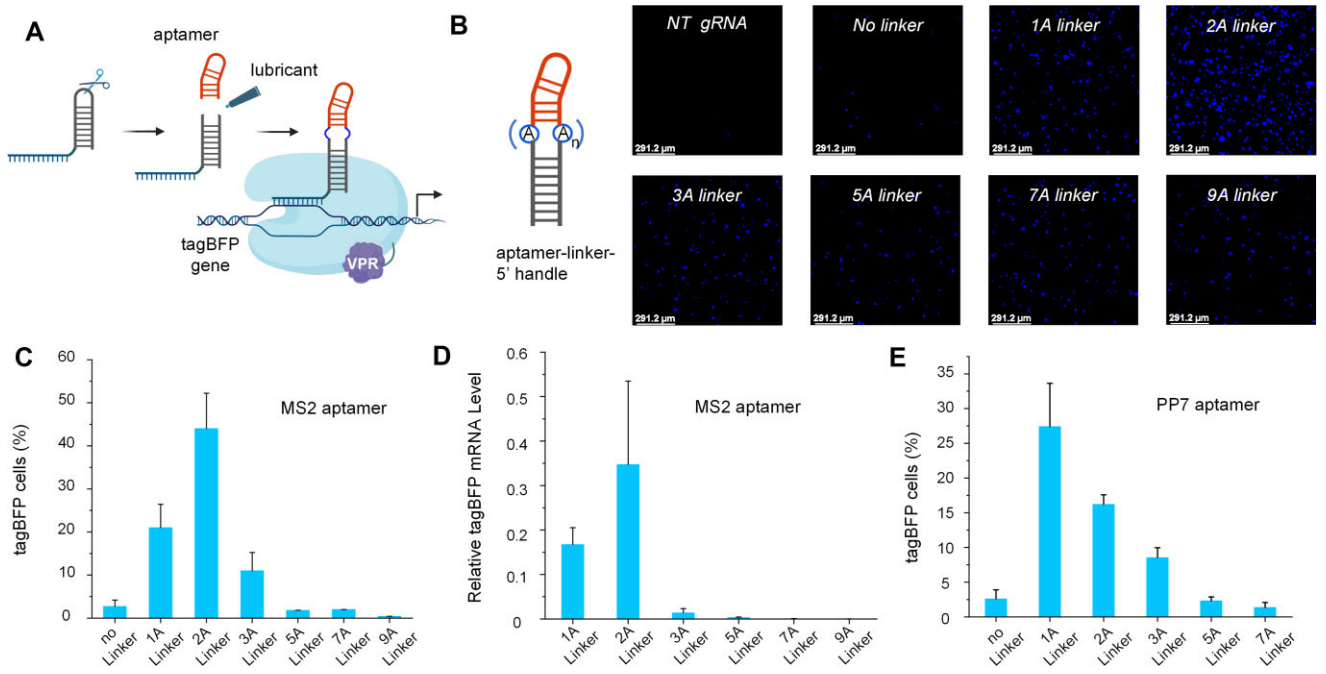

Figure 4. Embedding RNA aptamer motif on 5′ handle of gRNA. (**A**) The diagram shows that the 5′ handle region of the CRISPR–Cas12a gRNA enables the embedding of RNA aptamer motifs, such as the MS2 and PP7 aptamer motifs. (**B–D**) Optimization of the number of adenine bases between the MS2 element and the gRNA for CRISPR activity. In the confocal microscopy results, "NT gRNA" represents the nontarget gRNA and "No linker" represents the direct fusion of MS2 and the gRNA; scale bars: 291.2 μm. (**E**) Optimization of the length of the adenine base linker between the gRNA and the PP7 RNA aptamer. The tagBFP cells (%) represent the ratio of cells with tagBFP expression induced by different aptamer–gRNA sequences to cells with tagBFP expression induced by the normal gRNA–BFP. The error bars represent the standard deviation of three measurements.

cells cultured without theophylline (Fig. 5E and F). These findings strongly suggest that our theophylline-inducible PARC–Cas12a system can respond to external input signals in mammalian cells, thus altering cellular signal transduction and regulating cellular gene expression.

Discussion

In this study, we engineered a CRISPR–Cas12a system with a programmable proximity-activated guide RNA (PARC–Cas12a), providing novel insight into the integration of RNA engineering and type V CRISPR systems. A key contribution of our work is the demonstration of the successful splitting and reassembly of the AsCas12a gRNA. By analyzing the crystal structure of AsCas12a, we found that the loop region of the compact 5′ handle of the gRNA ("UCUU" sequence) is positioned in an open pocket-like structure in the Cas12a protein, where the four-base sequence "UCUU" is completely free of interactions with the amino acid side chains of Cas12a. We demonstrated that the gRNA could be split into two segments at the "UCUU" site in the 5′ handle, leading to transient loss of CRISPR activity. However, these segments were able to be reassembled through external means, such as nucleic acid hybridization or interactions with small molecules and aptamers, to restore CRISPR–Cas12a functionality. This mechanism underpins a novel method to control Cas12a activity and significantly expands the potential applications of CRISPR–Cas12a system (Fig. 1B).

Consequently, by introducing a trigger RNA and extending the ends of the split gRNA fragments to assemble a TC tile, we developed an RNA-inducible CRISPR–Cas12a system. In addition to exploring nucleic acid targets, we investigated the feasibility of constructing non-nucleic acid target-inducible PARC–Cas12a systems. By integrating small molecule aptamers into the split gRNA, we demonstrated two different activation strategies. In the ATP-inducible PARC–Cas12a system, the split ATP aptamer is directly connected to the split gRNA, with the fragments reassembled upon ATP binding to restore Cas12a activity. In the theophylline-inducible system, a riboswitch mechanism is exploited, wherein the theophylline aptamer brings the pseudosplit gRNA fragments into proximity, thus activating Cas12a. In this system, the target of interest functions as a switch to control the activity of CRISPR–Cas12a, while the results of Cas12a-mediated DNA cleavage can provide feedback on the concentration of the target molecule. This observation suggests that the system holds two important features: (i) the ability to allow qualitative and quantitative analysis of targets of interest through examining both the sequence and the amount of cleaved DNA, and (ii) the ability to employ the target of interest to control the activity of Cas12a, achieving stimulus-responsive or spatiotemporal control of gene regulation in cells.

On the basis of the above findings, the PARC–Cas12a system has potential for use in diagnostic applications. We verified the feasibility of a sensitive fluorescence strategy for detecting RNA and non-nucleic acid targets such as ATP, utilizing the *trans*-cleavage signal amplification capability of the PARC–Cas12a system. Comparisons with the CRISPR–Cas13a system revealed that the RNA-inducible PARC–Cas12a system has a LOD (112 amol) comparable to that of LbuCas13a. Both systems operate within the pM range. In addition, the PARC–Cas12a system cleaves DNA, whereas Cas13a directly degrades target RNA. This advantage allows the construction of an RNA detection array, where multiple split-crRNA groups target distinct regions

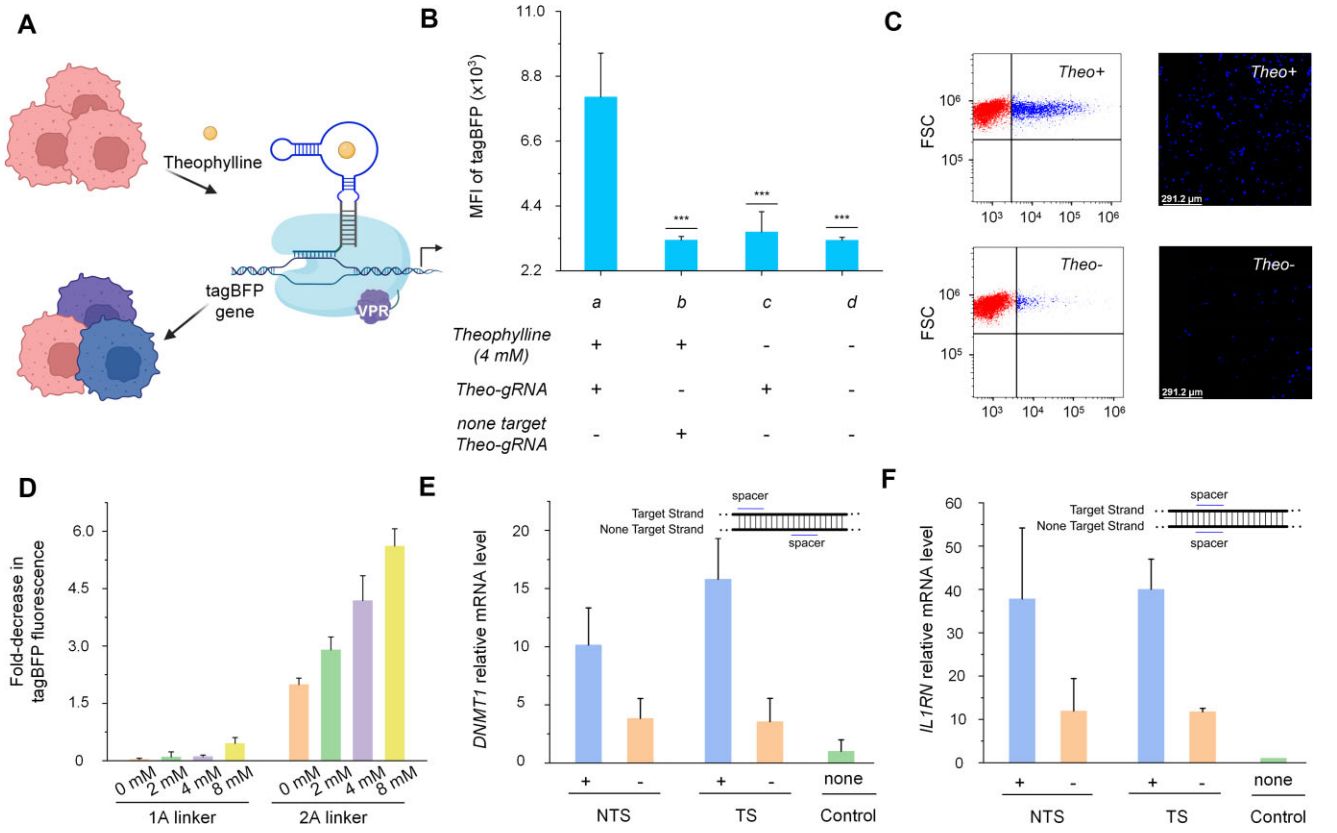

Figure 5. Theophylline-inducible PARC–Cas12a. (**A**) Schematic representation of a gene activation system constructed using a theophylline-inducible PARC–Cas12a design. (**B** and **C**) CRISPRa activity of gRNAs embedded with the theophylline aptamer in HEK293T cells. The mean fluorescence intensity of tagBFP with or without theophylline was determined via the flow cytometry. A nontargeting spacer was used as a control group. The scale bars in the confocal images represent 291.2 μm. (**D**) The expression level of tagBFP in HEK293T cells that responded to different concentrations of theophylline was measured via the flow cytometry. The presence of a double-A linker resulted in increased activation efficiency. (**E** and **F**) CRISPRa of the endogenous *DNMT1* and *IL1RN* genes. We designed two independent groups of spacers and assayed transcriptional activation via qRT-PCR. The lines on dsDNA gene represent the sequences of the spacers for the gRNA pair with either the template DNA strand (TS) or the nontemplate DNA strand (NTS). The control group lacked a gRNA. Reported data are the mean ± SD from three independent experiments. $***P < .001$ was calculated by Student's *t*-test (compared to theophylline-positive group).

of the same RNA molecule. By leveraging this property, the arrayPARC–Cas12a system achieves ultra-sensitive detection, accommodating over 10 detection units per RNA sample and reaching a remarkable LOD of 10 fM within 30 min. This innovative design overcomes the limitations of Cas13a and significantly enhances RNA detection performance. Besides, to fully actualize the multiplexing potential of the PARC–Cas12a system, we developed a new assay using metal-labeled DNA probes and streptavidin-coated magnetic beads (DMP–SMB). This method combines precise recognition and cleavage by PARC–Cas12a with metal labeling, rapid separation via magnetic beads, and accurate detection using the ICP-MS. The ICP-MS results demonstrated a strong linear correlation between the signal intensity and the RNA concentration, indicating that this method can reliably quantify RNA samples. The ability of the ICP-MS to distinguish isotopes of metal elements indicates that this strategy can potentially be used to analyze >10 different RNA species simultaneously.

Moreover, we extended the use of the PARC–Cas12a system for controllable gene regulation in cells. The initial test involved inducible gene knockout in *E. coli*. The presence of a trigger RNA activated the PARC–Cas12a system, leading to significant GFP plasmid cleavage and fluorescence reduction. We further explored the feasibility of the system for RNA-regulated CRISPRi via dCas12a. By designing trigger RNAs to assemble split gRNAs in *E. coli* cells, the capacity for multiplex gene regulation was tested by coexpressing the sfGFP and mRFP1 genes, with their transcription regulated independently and effectively by specific trigger RNAs. To expand the application of the PARC–dCas12a system for CRISPRi of endogenous genes, we introduced a gRNA spacer targeting the *lacZ* gene. Upon introduction of the trigger RNA of the PARC–dCas12a system, the *lacZ* mRNA level was significantly reduced. Further tests using endogenous RNAs, such as the sRNA RyhB, as trigger RNAs revealed that the PARC–Cas12a system can regulate bacterial gene expression in response to changes in the external environment as observed under stimulation by iron deficiency. These findings underscore the potential of the PARC–Cas12a system for complex gene regulatory networks and synthetic biological circuits in bacterial cells.

In mammalian cells, we successfully incorporated RNA aptamers into the gRNA at the "UCUU" split site. By adding adenine bases as linkers, we improved the compatibility of the engineered gRNAs with the Cas12a protein. This approach enabled the development of a theophylline-inducible PARC–Cas12a system that was able to regulate gene transcription in HEK293 cells. The dCas12a–VPR system was activated

by theophylline, leading to the upregulation of endogenous target genes such as *DNMT1* and *IL1RN*. This inducible system offers a versatile tool for controlling gene expression in complex eukaryotic systems, with considerable potential for applications in gene therapy and cellular engineering. Despite these promising results, a deeper understanding of the behavior of Cas proteins and gRNA assembly in mammalian cells is necessary, and will be highly important for the integration of RNA engineering and CRISPR–Cas technology. Expanding the range of small molecules and aptamers that can be used to induce CRISPR activity will broaden the applicability of the system. Future research should thus focus on refining RNA engineering techniques to develop highly tunable and responsive gRNA constructs. This effort involves exploring new RNA elements and regulatory sequences that can be integrated into the 5′ handle structure without compromising CRISPR activity.

In summary, we propose a new paradigm for integrating engineered RNAs with CRISPR–Cas12a system. The successful implementation of RNA-inducible and small molecule-inducible CRISPR systems in both prokaryotic and eukaryotic cells highlight the broad potential of the PARC–Cas12a system. Continued optimization and expansion of this system will pave the way for impactful biomedical applications, including applications in advanced diagnostics, gene therapy, and synthetic biology. We believe that additional CRISPR–Cas systems, such as the CRISPR–Cas13 system, can be used to develop programmable proximity-activated RNA engineering strategies, a possibility currently being explored by our group, leading to future innovations in gene editing and molecular diagnostics.

Acknowledgements

We would like to thank Professor Junjie Liu and Yangming Wang from Tsinghua University and Peking University for their invaluable guidance on the structure of the CRISPR–Cas12a system and plasmid construction. We would also like to thank Huasong Ai for his assistance with the EMSA experiments, Professor Zhi Xing from Tsinghua University for his help with the ICP-MS testing, and Lufeng Hu from Peking University for his assistance with the mammalian cell experiments. We thank Tiffany Norton, PhD, from American Journal Experts (https://www.aje.cn/) for editing a draft of this manuscript. The graphical abstract was created in BioRender (https://BioRender.com/i45q887).

Author contributions: Z.H., S.L., and J.D. performed the experiments and data analyses. Y.C., S.W., and Z.Y. contributed to the preparation of the materials. Z.H. and Z.L. designed the experiments. X.Z. and S.Z. assisted with article writing and *in vitro* experiments. Z.H., S.L., and J.D. wrote the manuscript. Z.H. and Z.L. supervised the project. Z.L. revised the manuscript and provided financial support for the project.

Supplementary data

Supplementary data is available at NAR online.

Conflict of interest

The authors declare nocompeting financial interest.

Funding

This work was supported by grants from the National Science and Technology Major Project of the Ministry of Science and Technology of China (2022YFF0710200). We thank the National Natural Science Foundation of China (22304007 and 22234001) for their support for this project. We thank the Beijing Municipal Natural Science Foundation [2252014]. Funding to pay the Open Access publication charges for this article was provided by the author.

Data availability

All raw data can be made available upon request.

References

1. Hsu PD, Lander ES, Zhang F. Development and applications of CRISPR–Cas9 for genome engineering. *Wiley Interdiscip Rev RNA* 2014;**157**:583–88.
2. Kaminski MM, Abudayyeh OO, Gootenberg JS *et al.* CRISPR-based diagnostics. *Nat Biomed Eng* 2021;**5**:643–56.
3. Katti A, Diaz BJ, Caragine CM *et al.* CRISPR in cancer biology and therapy. *Nat Rev Cancer* 2022;**22**:259–79.
4. Sander JD, Joung JK. CRISPR–Cas systems for editing, regulating and targeting genomes. *Nat Biotechnol* 2014;**32**:347–55.
5. Li J, Green AA, Yan H *et al.* Engineering nucleic acid structures for programmable molecular circuitry and intracellular biocomputation. *Nat Chem* 2017;**9**:1056–67.
6. Dykstra PB, Kaplan M, Smolke CD. Engineering synthetic RNA devices for cell control. *Nat Rev Genet* 2022;**23**:215–28.
7. Kim D, Kim J, Hur JK *et al.* Genome-wide analysis reveals specificities of Cpf1 endonucleases in human cells. *Nat Biotechnol* 2016;**34**:863–68.
8. Kleinstiver BP, Tsai SQ, Prew MS *et al.* Genome-wide specificities of CRISPR–Cas Cpf1 nucleases in human cells. *Nat Biotechnol* 2016;**34**:869–74.
9. Paul B, Montoya G. CRISPR–Cas12a: functional overview and applications. *Biomed J* 2020;**43**:8–17.
10. Chen JS, Ma E, Harrington LB *et al.* CRISPR–Cas12a target binding unleashes indiscriminate single-stranded DNase activity. *Science* 2018;**360**:436–39.
11. Xiong Y, Zhang J, Yang Z *et al.* Functional DNA regulated CRISPR–Cas12a sensors for point-of-care diagnostics of non-nucleic-acid targets. *J Am Chem Soc* 2020;**142**:207–13.
12. Lu S, Tong X, Han Y *et al.* Fast and sensitive detection of SARS-CoV-2 RNA using suboptimal protospacer adjacent motifs for Cas12a. *Nat Biomed Eng* 2022;**6**:286–97.
13. Feng W, Newbigging AM, Tao J *et al.* CRISPR technology incorporating amplification strategies: molecular assays for nucleic acids, proteins, and small molecules. *Chem Sci* 2021;**12**:4683–98.
14. Zhang Q, Gao X, Ho YP *et al.* Controllable assembly of a quantum dot-based aptasensor guided by CRISPR–Cas12a for direct measurement of circulating tumor cells in human blood. *Nano Lett* 2024;**24**:2360–68.
15. Yamano T, Nishimasu H, Zetsche B *et al.* Crystal structure of Cpf1 in complex with guide RNA and target DNA. *Cell* 2016;**165**:949–62.
16. Zetsche B, Gootenberg JS, Abudayyeh OO *et al.* Cpf1 is a single RNA-guided endonuclease of a class 2 CRISPR–Cas system. *Cell* 2015;**163**:759–71.
17. Li B, Zhao W, Luo X *et al.* Engineering CRISPR–Cpf1 crRNAs and mRNAs to maximize genome editing efficiency. *Nat Biomed Eng* 2017;**1**:0066.
18. Rozners E. Chemical modifications of CRISPR RNAs to improve gene-editing activity and specificity. *J Am Chem Soc* 2022;**144**:12584–94.

19. Oesinghaus L, Simmel FC. Switching the activity of Cas12a using guide RNA strand displacement circuits. *Nat Commun* 2019;**10**:2092.
20. Collins SP, Rostain W, Liao C *et al.* Sequence-independent RNA sensing and DNA targeting by a split domain CRISPR–Cas12a gRNA switch. *Nucleic Acids Res* 2021;**49**:2985–99.
21. Lin J, Wang WJ, Wang Y *et al.* Building endogenous gene connections through RNA self-assembly controlled CRISPR–Cas9 function. *J Am Chem Soc* 2021;**143**:19834–43.
22. Pelea O, Fulga TA, Sauka-Spengler T. RNA-responsive gRNAs for controlling CRISPR activity: current advances, future directions, and potential applications. *CRISPR J* 2022;**5**:642–59.
23. Moon SB, Kim DY, Ko JH *et al.* Improving CRISPR genome editing by engineering guide RNAs. *Trends Biotechnol* 2019;**37**:870–81.
24. Chang HY, Qi LS. Reversing the central dogma: RNA-guided control of DNA in epigenetics and genome editing. *Mol Cell* 2023;**83**:442–51.
25. Hu Z, Sun A, Yang J *et al.* Regulation of the CRISPR–Cas12a system by methylation and demethylation of guide RNA. *Chem Sci* 2023;**14**:5945–55.
26. Debiais M, Lelievre A, Smietana M *et al.* Splitting aptamers and nucleic acid enzymes for the development of advanced biosensors. *Nucleic Acids Res* 2020;**48**:3400–22.
27. Wrist A, Sun W, Summers RM. The theophylline aptamer: 25 years as an important tool in cellular engineering research. *ACS Synth Biol* 2020;**9**:682–97.
28. Femino AM, Fay FS, Fogarty K *et al.* Visualization of single RNA transcripts *in situ*. *Science* 1998;**280**:585–90.
29. Chen KH, Boettiger AN, Moffitt JR *et al.* RNA imaging. Spatially resolved, highly multiplexed RNA profiling in single cells. *Science* 2015;**348**:aaa6090.
30. Liu R, Zhang S, Wei C *et al.* Metal stable isotope tagging: renaissance of radioimmunoassay for multiplex and absolute quantification of biomolecules. *Acc Chem Res* 2016;**49**:775–83.
31. Massé E, Escorcia FE, Gottesman S. Coupled degradation of a small regulatory RNA and its mRNA targets in *Escherichia coli*. *Genes Dev* 2003;**17**:2374–83.
32. Konermann S, Brigham MD, Trevino AE *et al.* Genome-scale transcriptional activation by an engineered CRISPR–Cas9 complex. *Nature* 2015;**517**:583–88.
33. Hu LF, Li YX, Wang JZ *et al.* Controlling CRISPR–Cas9 by guide RNA engineering. *Wiley Interdiscip Rev RNA* 2023;**14**:e1731.

Received: December 12, 2024. **Revised:** January 3, 2025. **Editorial Decision:** January 4, 2025. **Accepted:** January 8, 2025